Agriculture, Ecosystems and Environment 242 (2017) 1–8

Contents lists available at ScienceDirect

Agriculture, Ecosystems and Environment

journal homepage: www.elsevier.com/locate/agee

Effect of vegetation type on microstructure of soil aggregates on the Loess Plateau, China

Dong Zhao[a,c], Mingxiang Xu[a,b,**], Guobin Liu[a,*], Luyang Ma[b], Shengmin Zhang[b], Tiqiao Xiao[d], Guanyun Peng[d]

[a] State Key Laboratory of Soil Erosion and Dryland Farming on the Loess Plateau, Institute of Soil and Water Conservation, Chinese Academy of Sciences and Ministry of Water Resources, Yangling, Shaanxi 712100, PR China
[b] Northwest A & F University, Yangling, Shaanxi 712100, PR China
[c] University of Chinese Academy of Sciences, Beijing 100049, PR China
[d] Shanghai Synchrotron Radiation Facility (SSRF), Shanghai Institute of Applied Physics, Chinese Academy of Science, Shanghai 201204, PR China

ARTICLE INFO

Article history:
Received 24 December 2016
Received in revised form 14 March 2017
Accepted 15 March 2017
Available online xxx

Keywords:
Aggregate pore
Micro-computed tomography
Soil organic matter
Soil texture
Vegetation restoration

ABSTRACT

Several types of vegetation restoration have been implemented on the Loess Plateau in China to control soil erosion and improve soil quality. Different revegetation types, however, have varying effects on soil structure; effects on the pore network of aggregates are especially not well understood. We used synchrotron-based high-resolution X-ray micro-computed tomography to quantify the microstructure of soil aggregates under four types of revegetation and an active cropland on the plateau. Five aggregates (3–5 mm) collected from the topsoil at each site were scanned at a voxel resolution of 3.25 μm, and the aggregate pore structure was visualized and quantified with ImageJ. Total porosities, >75 μm porosities, fractions of elongated pores, 3D mass fractal dimensions, and connectivity were higher and the numbers of pores, <75 μm porosities, the mean pore-shape factors, and the fractions of regular and irregular pores were lower in the revegetated sites than the control plot. Total porosities, macro-porosities, micro-porosities, fractions of regular pores, and 3D mass fractal dimensions differed significantly among the revegetated sites. We suggest that the fraction of elongated pores can be used as an important indicator for monitoring the recovery of soil structure. 3D mass fractal dimensions differed more than connectivity in the aggregates in the same samples, and thus could be a more sensitive indicator of changes in the pore network. Age and revegetation type both significantly affected the development of soil structure, but revegetation type was more important for the recovery of soil structure. We used a soil structural index (SSI) obtained by principal component analysis to assess the overall quality of soil structure. SSI values were higher in all revegetated sites than the cropland site and differed among the revegetated sites in the order: shrubland > grassland > woodland > pastureland. We recommend shrub plantation and natural grassland for the revegetation of degraded land on the Loess Plateau.

1. Introduction

Soil erosion is a worldwide problem with both social and environmental consequences (Duan et al., 2016). The restoration of vegetation in arid and semi-arid regions can increase the interception of rainwater and its retention in the soil (Sun et al., 2006). Revegetation has been widely used to control soil erosion and ecosystemic degradation (Bienes et al., 2016; Chen et al., 2010; Zhang et al., 2016). The Chinese government has initiated several projects for vegetation restoration on the Loess Plateau to conserve soil and water resources and restore damaged environments (Deng and Shangguan, 2012; Zhang and Shangguan, 2016). These projects have encouraged the conversion of cropland (particularly on steep slopes) to grassland, shrubland, or forest (Chen et al., 2007; Zhang et al., 2011). Proper adjustments of land use has increased the vegetation coverage on the plateau from 31.6% in 1999 to 56.9% in 2013, and the annual discharge of sediment from the Yellow River has been decreased to 0.2 billion tonnes, similar to historic levels (Chen et al., 2015; Wang et al., 2016).

* Corresponding author.
** Corresponding author at: State Key Laboratory of Soil Erosion and Dryland Farming on the Loess Plateau, Institute of Soil and Water Conservation, Chinese Academy of Sciences and Ministry of Water Resources, Yangling, Shaanxi 712100, PR China.
E-mail addresses: xumx@nwsuaf.edu.cn (M. Xu), gbliu@ms.iswc.ac.cn (G. Liu).

http://dx.doi.org/10.1016/j.agee.2017.03.014
0167-8809/

The structure of soil is central to its functioning, because it controls the fluxes and storage of water, gases, and nutrients and influences biological, physical, and chemical processes (Angers and Caron, 1998). The recovery of good soil structure by restoring vegetation is thus key to improving soil quality and fulfilling the essential functions of soil (Zhao et al., 2017). Revegetation practices can substantially change the physical and hydraulic properties of soil, including changes in organic matter content, porosity, hydraulic conductivity, and water retention (Kravchenko et al., 2011), and can affect soil structure in complex ways. In vegetation-restoration programs, forests and shrublands have improved soil structure more than grasslands (Zhang and Shangguan, 2016; Zhao et al., 2010). Evaluating the impact of vegetation recovery on soil structure is important for our understanding of the evolution of the ecological function of soil and can help the development of recommendations for eco-environmental reconstruction or rehabilitation.

X-ray computed tomography (CT), combined with image-analysis techniques, has recently been used to non-destructively study soil structure with a higher resolution and contrast and faster scanning than previous methods (Hu et al., 2016). X-ray CT scanning is also a unique tool for the 3D visualization and quantification of soil structure (Garbout et al., 2013; Zhou et al., 2012). For example, Luo et al. (2010) quantified 3D networks of soil macropores in various soil types and land uses in experimental columns using a medical CT scanner. Micro-CT, especially synchrotron radiation-based micro-computed tomography (SR-μCT), can enable researchers to quantify the internal structures of aggregates with a resolution of one to several microns (Ma et al., 2015; Peth et al., 2008; Zhou et al., 2016). Zhou et al. (2013) used SR-μCT to compare the effect of long-term organic and inorganic fertilization on the pore structure of aggregates (approximately 5 mm) and found that organic fertilization could improve pore network but the latter was ineffective.

Zhou et al. (2012) indicated that the pore system was improved after vegetation restoration on eroded bare land in the erodible red soil region of China. We visualized and quantified the microstructures of soil aggregates using SR-μCT in a previous study on the Loess Plateau over 32 years of revegetation (grassland) (Zhao et al., 2017). Revegetation significantly affected pore-size distribution, number of pores, and pore shape and facilitated the connection and development of aggregate microstructures by increasing the fractal dimension, anisotropy, and pore connectivity. Such information about aggregate pore characteristics would deepen our understanding of the mechanisms that determine soil structure (Kravchenko et al., 2011), but those studies were only concerned about one simple type of revegetation, and few studies have focused on the changes in aggregate microstructures by revegetation practices using SR-μCT. Evaluating the impacts of more types of revegetation (e.g. afforestation and artificial grassland) on the CT-measured characteristics of aggregate pores is therefore essential. A comparison of the impact of different revegetation types on aggregate microstructures is especially urgently needed, because it could be of guiding importance for the establishment of practices of adaptive ecological restoration in eco-fragile regions.

We hypothesized that vegetation restoration would improve the microstructure of soil aggregates and that different types of restoration could produce observable differences in the characteristics of aggregate pores. The objectives of this study were to: (i) evaluate the effects of different types of vegetation restoration on pore characteristics (number of pores, porosity, and pore morphological parameters), and (ii) determine the optimal type of vegetation for the recovery of soil structure on the Loess Plateau.

2. Materials and methods

2.1. Study sites

The sampling site was in the Zhifanggou Watershed in Ansai County, Shaanxi Province, northern Loess Plateau, China (109°13′46″–109°16′33″E, 36°43′11″–36°46′25″N; 1010–1431 m a.s.l.; 8.27 km^2). The area has hilly gullied loessial landscape with a temperate and semi-arid climate. The area's mean annual temperature is 8.8 °C (min −23.6 °C and max 36.8 °C) and annual evaporation ranges from 1010 to 1400 mm. The mean annual precipitation is 505 mm (1970–2006), 70% of which falls in the period of July to September (Zhao et al., 2017). The soil is a Calcaric Cambisol (FAO, 1990), originating from wind deposits and characterized by weak cohesion, high infiltrability, and low water retention (Fu et al., 2010).

The watershed is located in an ecotone of forest and grass. The vegetation has been widely rebuilt in this area in recent decades to remedy the problem of soil degradation (Zhang et al., 2011). Most of the cultivated land on the slopes has been gradually abandoned for natural and artificial revegetation. The main species used for artificial vegetation have included *Robinia pseudoacacia* L. (woodland), *Caragana korshinskii* Kom. and *Hippophae rhamnoides* L. (shrubland), and *Medicago sativa* L., *Astragalus adsurgens* Pall., and *Panicum virgatum* L. (grassland). Naturally restored areas contain *Artemisia capillaris* Thunb., *Heteropappus altaicus* (Willd.) Novopokr., and *Artemisia sacrorum* Ledeb.

2.2. Experimental design and soil sampling

We chose four typical types of vegetation restoration as the experimental sites: (1) pastureland (**PL**) based on alfalfa (*M. sativa*), which was annually drilled or broadcasted in April and harvested in late July; (2) grassland (**GL**) consisting of an endemic natural grass (*A. sacrorum*), which was allowed to naturally recolonize abandoned cropland; (3) shrubland (**SL**) based on Korshinsk peashrub saplings (*C. korshinskii*) planted in a 1.0 × 1.0 m grid; and (4) woodland (**WL**) consisting of black locust trees (*R. pseudoacacia*) planted 2.5–3 m apart in rows. A cropland (**CK**) planted with millet (*Setaria italica* L.) was selected as a reference site. All plants had grown for nearly 15 years under semi-arid conditions, without irrigation, fertilization, or disturbance after planting, except for the PL and CK sites. The CK site was annually tilled to a depth of 20 cm

Table 1
Detailed information for the experimental plots.

Plot name	Latitude (N)	Longitude (E)	Altitude (m)	Slope (°)	Slope Aspect	Dominant species
CK	109°14′35″	36°44′39″	1266	19	NE	*Setaria italica* L.
PL	109°14′57″	36°44′22″	1194	18	N	*Medicago sativa* L.
GL	109°16′31″	36°44′02″	1289	21	NE18°	*Artemisia sacrorum Ledeb.*
SL	109°15′29″	36°43′54″	1292	23	N	*Caragana korshinskii Kom.*
WL	109°15′20″	36°43′57″	1279	25	NE10°	*Robinia pseudoacacia* L.

Note: CK – slope cropland; PL – Pastureland; GL – Grassland; SL – Shrubland; WL – Woodland.

in May, and the aboveground part of millet was harvested in late August (Fu et al., 2010). The alfalfa and millet aboveground biomass was harvested and removed each year. Chemical fertilizers have been applied to the cropland at 120 kg ha^{-1} N and 60 kg ha^{-1} P_2O_5 annually, as recommended by the local agricultural service (Fu et al., 2010). The sampling sites were all near the tops of loessial mounds and differed little in topography and previous farming practices. Detailed site information is shown in Table 1.

Five plots were set up in each vegetation type in July 2014 for sampling. The size of the plots was based on the size of the communities: 20 × 20 m plots in WL, 5 × 5 m plots in SL, and 2 × 2 m plots in PL, GL, and CK (Deng et al., 2016). The distance between any two plots was >500 m, so the plots can be considered as true replicates of the total experimental area (Marriott et al., 1997). Topsoil samples (0–15 cm depth) were taken at five points in each plot and bulked and thoroughly mixed to make one composite sample for each replicate plot. Disturbed soil samples were manually broken into small pieces (<8 mm) and air-dried at room temperature. Undisturbed soil cores were collected at three points in each plot using a soil bulk sampler with a stainless steel cutting ring 5.0 cm in diameter and 5.0 cm long for measuring bulk density. Three samples of roots (0–15 cm depth) were collected in the center of each plot using a 9-cm diameter root auger (Deng et al., 2016). The roots were manually removed from the soil and oven-dried for measuring mass density. The fine roots were too few to detect from CK soil, because the sampled soil was bulk soil and few residual roots were left in soil after the intensive cultivation.

2.3. Analysis of soil properties

Air-dried subsamples were sieved through 2-mm and 0.25-mm screens, and prepared for particle-size and chemical analyses, respectively. Soil texture was measured using the Mastersizer 2000 method (Malvern Instruments Ltd, Malvern, UK), and soil organic matter (SOM) content was measured using potassium dichromate oxidation (Soil Survey Laboratory Methods Manual, 2004). Aggregates 3–5 mm in diameter obtained by passing subsamples through a 5-mm sieve were selected for testing aggregate stability using the fast-wetting treatment as described by Le bissonnais (1996), expressed as the mean weight diameter (MWD).

2.4. CT scanning and image processing

As bean time is limited, five aggregates (3–5 mm in diameter) were randomly selected from each sample for CT scanning. The soil aggregates were scanned using SR-μCT at beam line BL13W1 at the Shanghai Synchrotron Radiation facility. Slices were reconstructed from the radiographs and image format was converted, generating a stack of at least 550 2D images in 8-bit type, with a resolution of 3.25 μm in all three directions.

The images were processed, visualized, and quantified using the open-source program ImageJ, ver. 1.48 v (Rasband, 1997–2014). A region of interest of 500 × 500 × 500 voxels (i.e. 1.625 × 1.625 × 1.625 mm^3), representing an inscribed cube of an aggregate, was extracted from the central part of each image to avoid edge effects. The grayscale slices were segmented using the automatic Otsu thresholding algorithm (Garbout et al., 2013; Zhao et al., 2017), producing binary images from the original grayscale images (Fig. 1). The characteristics of the pore structure (i.e. total number of pores, porosity, and pore-size distribution) of the 3D images were obtained, and the pores were categorized into four size classes based on their equivalent diameter: <30, 30–75, 75–100, and >100 μm (Ma et al., 2015). A detailed description of these procedures is provided in Zhao et al. (2017).

2.5. Analysis of pore morphology

The pore-shape factor (F) was classified as regular (F ≥ 0.5), irregular (0.2 < F < 0.5), or elongated (F ≤ 0.2) according to the method of Zhou et al. (2012). The 3D mass fractal dimension (FD) and connectivity index (the volumetric Euler-Poincaré characteristic, hereafter Euler number, or E_V) were calculated using the

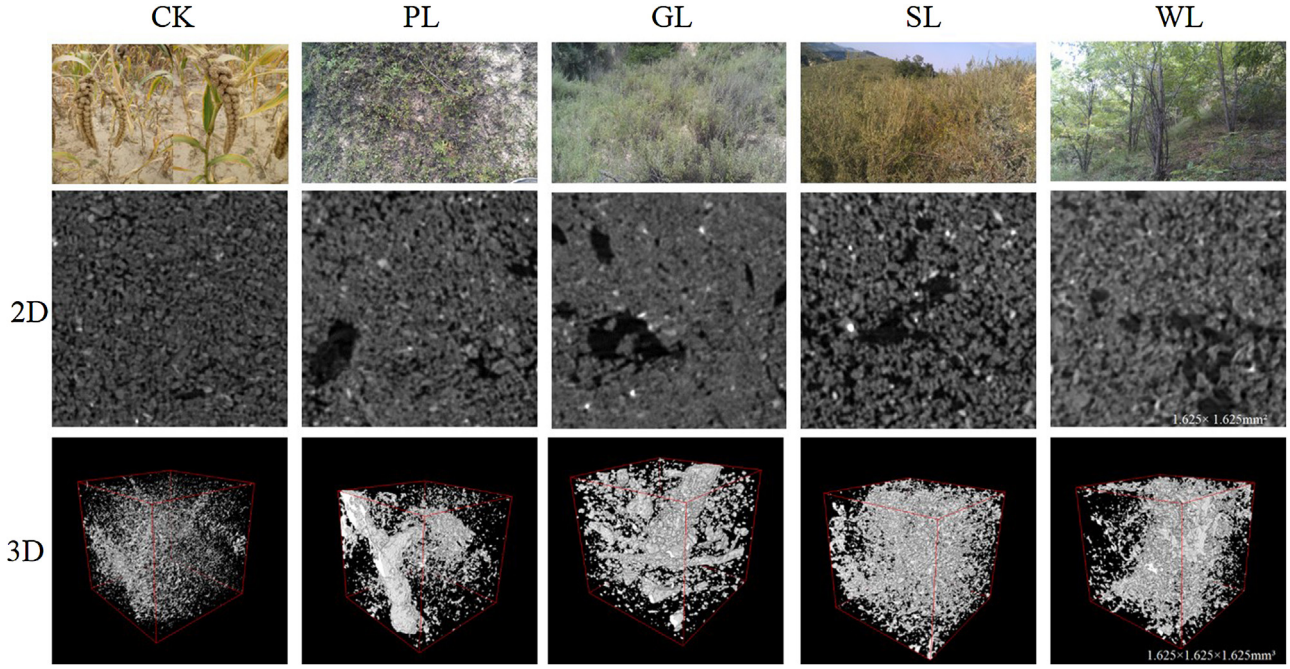

Fig 1. Photos and representative 2D and 3D structures of soil aggregates under different vegetation types. Note: CK – control plot; PL – Pastureland; GL – Grassland; SL – Shrubland; WL – Woodland.

Table 2
The characteristics of soil and restoration vegetation.

	Soil properties						Vegetation properties	
	Sand (%)	Silt (%)	Clay (%)	SOM(g kg^{-1})	BD(g cm^{-3})	MWD(mm)	Coverage (%)	RMD (g m^{-2})
CK	59.7 ± 3.5 a	29.6 ± 3.3 a	10.7 ± 0.8 ab	4.0 ± 1.1 c	1.26 ± 0.01 a	1.03 ± 0.33 c	78.2 ± 4.3 ab	–
PL	61.6 ± 1.8 a	26.8 ± 1.3 a	11.5 ± 0.6 a	5.9 ± 1.0 bc	1.25 ± 0.09 a	1.58 ± 0.29 b	76.8 ± 4.0 ab	93.9 ± 17.9 d
GL	64.0 ± 5.0 a	25.8 ± 3.6 a	10.1 ± 1.4 ab	7.5 ± 1.7 ab	1.09 ± 0.06 b	2.19 ± 0.21 a	72.4 ± 7.2 b	194.9 ± 29.1 b
SL	65.2 ± 3.5 a	25.2 ± 2.7 a	9.5 ± 1.0 b	8.3 ± 2.4 a	1.10 ± 0.06 b	2.13 ± 0.36 a	82.8 ± 3.7 a	269.1 ± 33.2 a
WL	62.9 ± 5.7 a	27.0 ± 4.3 a	10.1 ± 1.4 ab	6.5 ± 1.9 ab	1.14 ± 0.02 b	1.83 ± 0.13 ab	60.2 ± 8.3 c	146.8 ± 24.3 c

Note: SOM – soil organic matter; BD – bulk density; MWD – mean weight diameter; RMD – root mass density. Results are given as mean ± SD. Different letters following values among different vegetation types indicate significant difference at the $P < 0.05$ level (LSD).

ImageJ BoneJ plug-in to evaluate the complexity and connectivity of the pore networks inside the aggregates (Doube et al., 2010). The larger the FD, the higher the complexity of the pore system, opposite to E_V. The methodological details of the image analysis for deriving F, FD and E_V are described elsewhere (Dal Ferro et al., 2013; Zhao et al., 2017).

2.6. Developing the soil structural index

Soil structural quality can only be assessed using several (rather than single) properties that are sensitive to management-induced changes in soil processes and associated functions (Bastida et al., 2006; Raiesi and Kabiri, 2016). The soil structural index (SSI), combining structural properties into a single index, is provided as a better indication of the quality of soil structure for quantitatively comparing vegetation types. The higher the SSI, the better the soil structure. The SSI was determined in three steps: (i) selecting appropriate properties, (ii) transforming and weighting the properties, and (iii) integrating all scores into one overall value (Raiesi and Kabiri, 2016; Zhang et al., 2011).

A principal component analysis (PCA) was used to screen the most appropriate indicators. Principal components (PCs) with eigenvalues ≥1 were selected, because they could best explain the variability. Only the variables within 10% of the highest weighted loading were selected for indexing for each PC (Andrews et al., 2002). Correlation analysis was used to identify any redundant variables for reducing the number of variables. The uncorrelated indicators were then each considered important and were thus retained in the SSI; if indicators were strongly correlated, the indicator with the highest weighted loading (absolute value) was selected for the SSI (Sinha et al., 2009). Total porosity (TP), SOM content, and mean F (F_M) were the properties eventually selected from the PCs for inclusion in the SSI (see Appendices A–C for this procedure of selecting appropriate properties).

To transform the indicators into unitless combinable scores (S), indicating their contribution to soil structural quality, we used a sigmoidal curve to describe this target (Sinha et al., 2009; Zhang et al., 2011):

$$S = a/\left(1 + (x/x_o)^b\right) \quad (1)$$

where x is the value of the pore parameter, x_o is the average value of each pore parameter, a is the maximum score of the pore parameter (in this case, $a = 1$), and b is the slope. Two types of scoring functions were generated: a 'more is better curve' and a 'less is better curve' for all proposed properties, with slopes of −2.5 and 2.5, respectively.

The transformed indicator data were weighted based on the results of the PCA. Under a PC, weighting factors for the uncorrelated indicators were equal to the ratio of its variance with total variance, and the ratio was divided among the correlated indicators. The weighting factors were then standardized to unity (Armenise et al., 2013; Masto et al., 2008).

The SSI values were calculated after the indicators were scored and weighted as:

$$\mathrm{SSI} = \sum_{i-1}^{n} W_i S_i \quad (2)$$

where W_i is the calculated weight of each indicator, S_i is the indicator score, and n is the number of indicators.

2.7. Statistical analyses

The results are expressed as means ± standard deviations. Significant differences in soil properties and pore characteristics among the sites were analyzed with a one-way ANOVA and Fisher's test, calculated at $P = 0.05$. Correlation analysis, scoring, and the PCA were conducted to evaluate the SSI under different vegetation covers. All statistical analyses were carried out with SPSS version 20.0 (SPSS Inc., Chicago, USA).

3. Results

3.1. Soil and vegetation properties

Many soil and vegetation properties differed substantially among the sites after 15 years of vegetation restoration (Table 2). SOM content among the land covers was in the order: SL > GL > WL > PL > CK. Bulk densities were significantly lower in all revegetated sites than in CK, except PL. MWD, the most important indicator of aggregate stability, was highest in GL and SL, which did not differ from each other, followed by WL, PL, and CK. The texture of the surface soil, however, did not differ significantly among the sites ($P > 0.05$), except in PL and SL. Vegetation coverage was lowest (60%) in WL and was >72% in the other sites. Fine-root mass density differed markedly among the revegetated sites ($P < 0.05$) and was highest (269.1 g m^{-2}) in the surface soil in SL and lowest (93.9 g m^{-2}) in PL.

3.2. Porosity, number of pores, and pore-size distribution of the aggregates

The total porosity, total number of pores, and pore-size distribution of the aggregates in the five sites are shown in Fig. 2. The aggregate pores <3.25 μm could not be distinguished due to the limited resolution of the images. Total porosities of the aggregates differed substantially among the sites and were approximately 21, 43, 68, and 35% higher in PL, GL, SL, and WL, respectively, than in CK. In contrast, the total numbers of pores were significantly lower in the revegetated sites ($P < 0.05$) than CK but did not differ significantly among themselves ($P > 0.05$).

Pore-size distribution differed significantly among the five sites (Fig. 2). The 2D and 3D images of the aggregates indicated a clear tendency of modifications in microstructure in the various sites (Fig. 1). The >100 μm porosities were much higher in the

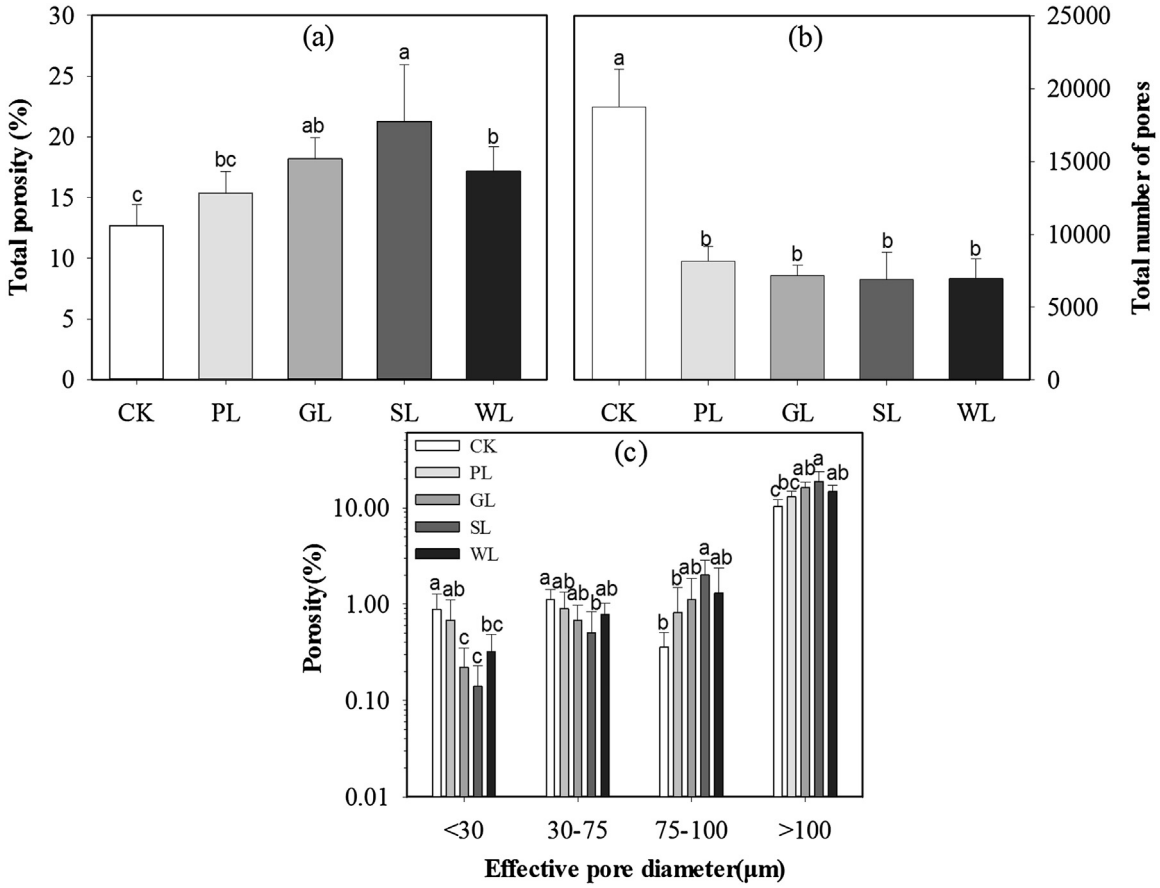

Fig. 2. Total porosity (a), total number of pores (b) and pore size distributions (c) of soil aggregates from the different treatments. Note: Different lower-case letters above the bars indicate significant differences among different vegetation types ($P < 0.05$). Error bars indicate standard errors.

revegetated sites than the control site, similar to the higher total porosities, in the order: SL > GL = WL > PL. Porosities for diameters 75–100 μm were slightly higher in the revegetated sites than the control site, but the difference was significant only for SL compared to PL and CK ($P > 0.05$). The revegetated sites also had more large pores than the control site (Fig. 1). The <30 and 30–75 μm porosities, however, tended to vary oppositely to that of the >100 and 75–100 μm porosities. The >100 μm porosities, accounting for more than 81–89% of the total porosities, were generally markedly higher than the <30, 30–75, and 75–100 μm porosities ($P < 0.05$).

3.3. Morphology of the aggregate pores

The variation of pore morphology within individual aggregates from the sites is shown in Fig. 3. The fraction of elongated pores was significantly higher in the revegetated sites than CK ($P < 0.05$) and was highest in SL and lowest in PL. Visual observations indicated that the aggregates in the revegetated sites also had more elongated pores (Fig. 1). In contrast, the fractions of regular and irregular pores were lower in the revegetated sites than CK. Mean F (F_M) ranged from 0.61 in CK to 0.51 in SL, similar to the fractions of regular pores.

FD differed significantly among all sites (Fig. 3). FD ranged between a maximum of 2.86 and a minimum of 2.77 in the order: SL > GL = WL > PL > CK. The connectivity (lower E_V) of the aggregates was higher at the revegetated sites than CK ($P < 0.05$), although E_V was similar among the four revegetated ecosystems ($P > 0.05$).

3.4. SSI

The means of the chosen properties, their type of scoring curve, and their weights are detailed in Table 3. The final normalized SSI equation was calculated as:

$$SSI = 0.71 \times S_{TP} + 0.17 \times S_{SOM} + 0.12 \times S_{FM} = 0.71 \times [1/(1 + (x_{TP}/16.94)^{-2.5}] + 0.17 \times [1/(1 + (x_{SOM}/6.44)^{-2.5}] + 0.12 \times [1/(1 + (x_{FM}/0.56)^{2.5}]$$

where x is the measured value for the subscripted variable. The results of the SSI for the sites using Eq. (4) are shown in Fig. 4. The SSI values could be grouped into three categories: (1) high SSI (>0.50), GL (0.54) and SL (0.62); (2) intermediate SSI (0.40–0.50), PL (0.44) and WL (0.50); and (3) low SSI (<0.40), CK (0.32).

4. Discussion

Vegetation restoration can modify soil-pore networks and thereby affect soil-water dynamics and balance (Zhao et al., 2010). The soil aggregates in CK had a dense structure with abundant small pores and microcracks, whereas the aggregates in the revegetated sites had a more porous structure with many interconnected large pores (Fig. 1). The quantification of the pore system, including total porosity, pore-size distribution, and pore morphology, indicated that the aggregate microstructures in the revegetated sites were more developed and porous (Figs. 2 and 3), consistent with the findings by Zhou et al. (2013). These observations were also supported by a previous study on the same watershed (Zhao et al., 2017), which suggested that the

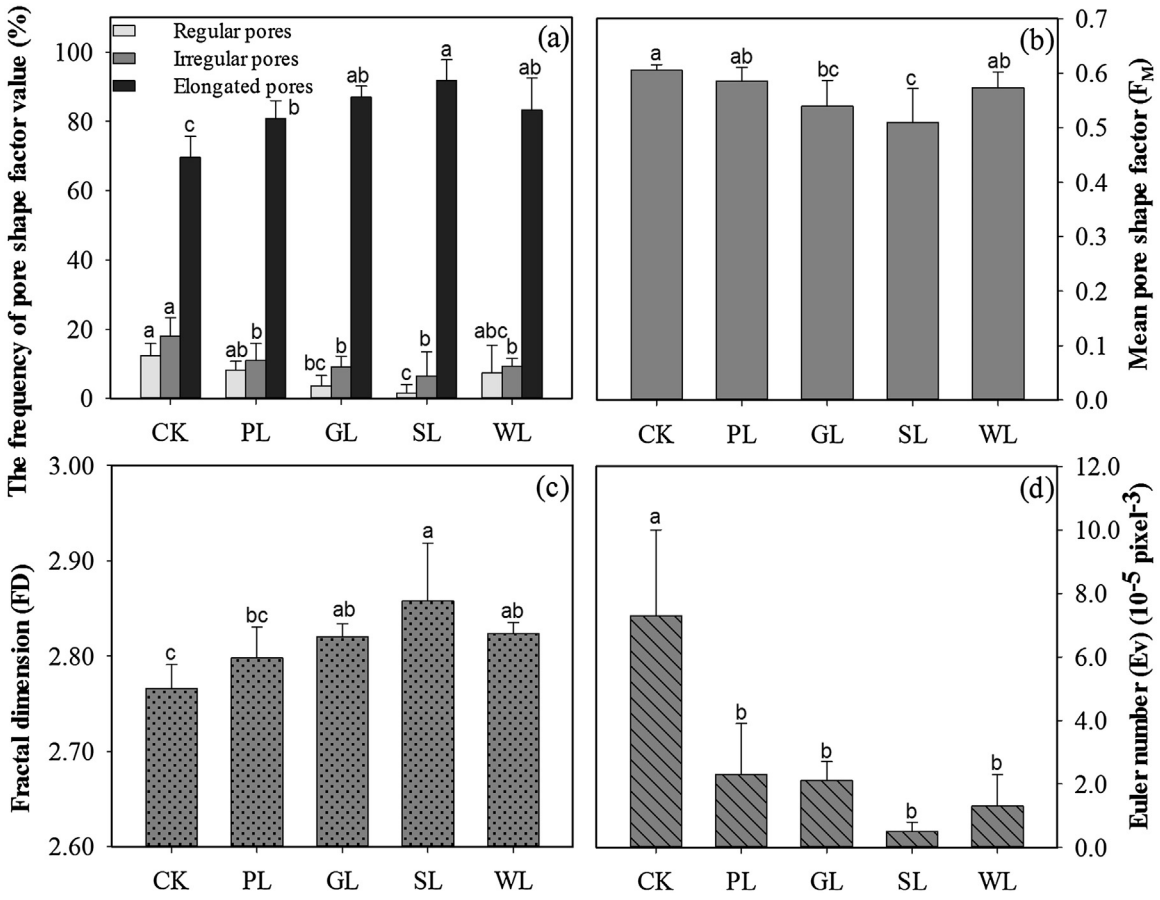

Fig. 3. Pore shape distribution (a), mean pore shape factor (b), fractal dimension (c) and Euler number (d) of soil aggregates in different treatments. Note: Different lower-case letters above the bars indicate significant differences among different vegetation types ($P < 0.05$). Error bars indicate standard errors.

Table 3
Parameters for scoring curves and weights.

		TP	SOM	F_M
1	Curve type	More is better	More is better	Less is better
2	Mean(x_0)	16.94	6.44	0.56
3	Slope(b)	−2.50	−2.50	2.50
4	R^2	0.987	0.970	0.998
5	Sig.	0.000**	0.000**	0.000**
6	Weight	0.55	0.13	0.09
7	Normalized weight	0.71	0.17	0.12

Note: TP – Total porosity; SOM – soil organic matter; F_M – mean shape factor. R^2 – correlation coefficient of regression equation; Sig. – significant relationships between measured values and calculated scores; ** $P < 0.01$.

improved aggregate microstructure by vegetation restoration could be due to the absence of tillage and an increase in the root system. Vegetation restoration contributed to the accumulation of SOM from the input of biomass (Deng et al., 2016); SOM can bind micro-aggregates, preventing the formation of microcracks but helping the formation of aggregate pores, therefore leading to fewer small pores and increasing porosity (Kravchenko et al., 2011). Additionally, the cropland did not contain vegetation before seeding, and the plant species for revegetation had already begun growing during that growing season. The longer active growing season may have thus contributed to the improvement of the root system and soil biological activity, thereby promoting greater porosity (Udawatta et al., 2006).

Udawatta et al. (2008) found that the parameters of soil porosity were more favorable in a natural than an artificial grassland and in a cropland, and Hu et al. (2016) suggested that shrubland soils had higher porosity and developed deeper and longer macropores than grassland soils. These results were, in part, consistent with the conclusions of our study. Roots can exploit cracks, voids, and large pores or enlarge smaller pores by their exploratory capability (Clark et al., 2003). The total porosity and the >100 μm porosity were both significantly positively correlated with root biomass in the present study (Appendix C), indicating that greater root development may create more large pores and increase porosities and macro-porosities (Hu et al., 2016; Udawatta et al., 2008). Udawatta et al. (2006) stated that the differences of

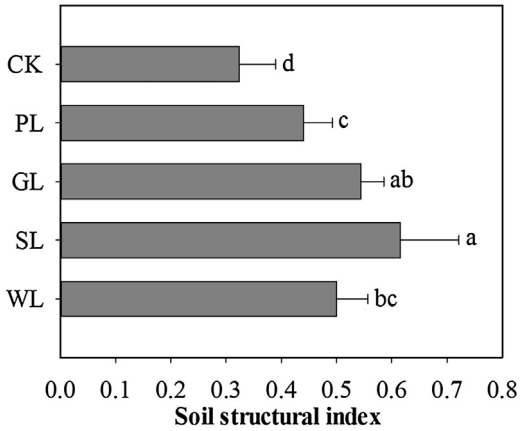

Fig. 4. Soil structural index (SSI) of different vegetation types. Note: Different lower-case letters next to the bars indicate significant differences among different vegetation types ($P < 0.05$). Error bars indicate standard errors.

porosity between two buffer patterns (tree and grass) were attributed to the differences in root activity, support our findings. The differences in aggregate porosities among the types of revegetation may also be attributed to organic matter, which would increase soil biological activity, thereby further facilitating pore development (Hu et al., 2016). In addition, the alfalfa in PL was harvested for stock feed each year. Soil disturbance would reduce air permeability and pore continuity and increase the destruction of aggregates (Hu et al., 2016), which may have been another cause of the lower porosity in PL than the other revegetated sites.

Different land covers can also have different impacts on pore shape. The fraction of elongated pores was much higher in the aggregates in the revegetated sites (average 86%) than the control site (70%). Dal Ferro et al. (2012) reported contrasting effects of management practices; pore shape differed little among different treatments, and irregularly shaped pores dominated all soil samples. These contradictory results are likely due to the different soil types and land uses. Elongated pores, which are important for root penetration and the storage and transmission of water and gases, are defined as transmission pores, ranging from 50 to 500 μm (Pagliai et al., 2004). These transmission pores play a vital role both in soil–water–plant relationships and in maintaining good soil structure (Bhattacharyya et al., 2006). The >100 μm porosity was significantly correlated positively with the fraction of elongated pores but negatively with the fraction of regular and irregular pores (Appendix C), indicating that the large pores were more elongated. Our findings also support those by Ma et al. (2015), who reported that the >100 μm porosity was more sensitive to the fraction of elongated pores. Total porosity had the same trend as the elongated pores (Figs. 2 and 3), indicating the increase in total porosity could be ascribed to the increase in the fraction of elongated pores (Pagliai et al., 2004). The fraction of elongated pores may also have contributed to the increase in complexity and connectivity of the pore network, supported by the significant positive and negative correlations with FD and E_V, respectively. The recovery of soil structure can thus be identified by an increase in the proportion of elongated pores.

This study also quantified the overall irregularity and connectivity of the pore structure using FD and E_V, respectively. FD was higher (2.83vs 2.77, Fig. 3c) and E_V was lower (1.6×10^{-5} vs 7.3×10^{-5} pixel^{-3}, Fig. 3d) in the revegetated sites than CK, indicating that the pore network became more intricate and continuous, which would facilitate infiltration, impede erosion, and stabilize the soil structure (Bienes et al., 2016; Dal Ferro et al., 2013). The differences in FD in the soil aggregates were nevertheless larger than that in E_V in the same samples, indicating that FD was more sensitive to the changes of the pore network. De Gryze et al. (2006) similarly proposed quantifying soil-pore systems using mass fractal dimensions rather than variograms. Our findings are also in accordance with those by Katuwal et al. (2015) who suggested that the Euler number was not a good measure of the connectivity of macropores between samples. Conversely, Dal Ferro et al. (2013) suggested that E_V was a more sensitive indicator than FD for identifying the effects of management practices. These discrepant conclusions were most likely due to the different resolutions of the tomographic images and to the thresholding methods. The development of a new widely accepted and morphologically based method of segmentation would therefore greatly help to reduce the limitations of structural analyses (Garbout et al., 2013; Zhou et al., 2013).

These CT-measured pore properties could not only reflect the evolution of soil structure during vegetation succession (Zhao et al., 2017), but could also identify the differences of aggregate microstructure between different revegetation types. Both age and vegetation types significantly affected the development of soil structure, but the pore parameters of SL aggregates was higher than that after 23 years of grass restoration and the pore parameters of aggregates in the grassland restored for six years was almost identical to that of the PL aggregates, indicating that the revegetation pattern had more influence than restoration age on the development of soil structure. The inappropriate vegetation type would not restore soil structure to a high level in a short time period, eventually affecting the benefit of soil and water conservation. Suitable plant species for revegetation should therefore first be identified, especially for the recovery of soil structure in degraded soil.

The above pore parameters identified differences in some aspects of the soil-structure network, but they may be biased and insufficiently comprehensive to indicate the overall change in soil structure because of the complex nature of soil (Zhang et al., 2011). The SSI was established based on the integrated soil-quality method (Sinha et al., 2009; Zhang et al., 2011) to evaluate the physical structural quality of different types of revegetation. The structural properties we chose were total porosity, F_M, and SOM content. Total porosity is a key attribute of soil structure that affects the ability to transport water and thereby influences the loss of nutrients in runoff and has thus been widely used as a measure of aeration and infiltration capacity of soil (Udawatta et al., 2008; Udawatta and Anderson, 2008; Zhang and Shangguan, 2016). F_M is a measure of the geometry of pores and their channels associated with the stability and heterogeneity of aggregates (Papadopoulos et al., 2009); F_M may also be a good indicator of the general pore system. SOM content has also become an indicator of soil structural quality, because it plays a vital role in the formation and preservation of pores (Hu et al., 2016). These selected properties can therefore generally be regarded as good indicators of soil structural quality and are thus important for choosing the plant species most suitable to restore eroded soils (Zhang et al., 2011). The SSI values indicated that these four types of revegetation had better soil structural quality relative to CK (Fig. 4). The higher SSI values suggest that conversions from cropland to shrubland or native grassland should be encouraged for restoration. Chen et al. (2007) and Chen et al. (2010) also highly recommended shrub plantation and native grassland for landscape restoration in semi-arid loessial hilly areas. These two types of vegetation can sequester more soil carbon and conserve more soil water, thereby facilitating the control of soil erosion and recovery of soil functions.

5. Conclusions

We assessed aggregate structure under different restored vegetation covers and an active cropland using SR-μCT in combination with image analysis. The 2D and 3D aggregate morphology, along with the quantitative pore parameters, indicated that all revegetation types had better aggregate microstructure compared to the control. Differences in the pore properties among the revegetated sites may be attributed to differences in root systems and organic carbon content. We suggest that the recovery of soil structure can be identified by an increase in the proportion of elongated pores due to their importance in soil functions associated with the transport and storage of water and oxygen. Both age and revegetation type significantly affected the development of soil structure, but revegetation type was more important for the recovery of soil structure. This study also supported earlier research on the efficiency of native grass and shrubs in revegetation on the Loess Plateau. The results of our study provide a helpful reference for assessing the soil functions associated with soil microstructures and highlight the importance of selecting suitable plant species for improving the physical quality of soil.

Acknowledgments

We gratefully acknowledge the BL13W1 beam line of the Shanghai Synchrotron Radiation Facility for supporting the CT scanning. Special thanks are given to Dr. Hu Zhou for his assistance with image analysis. We also thank Editor Yong Li and two anonymous reviewers for their constructive comments on the manuscript. This work was sponsored by the Key Research Program of the Chinese Academy of Sciences (Grant numbers: KJZD-EW-TZ-G10) and the National Natural Science Foundation of China (Grant numbers: 41171422).

Appendix A. Supplementary data

Supplementary data associated with this article can be found, in the online version, at http://dx.doi.org/10.1016/j.agee.2017.03.014.

References

Andrews, S.S., Karlen, D.L., Mitchell, J.P., 2002. A comparison of soil quality indexing methods for vegetable production systems in northern California. Agric. Ecosyst. Environ. 90, 25–45.
Angers, D.A., Caron, J., 1998. Plant-induced changes in soil structure: processes and feedbacks. Biogeochemistry 42, 55–72.
Armenise, E., Redmile-Gordon, M.A., Stellacci, A.M., Ciccarese, A., Rubino, P., 2013. Developing a soil quality index to compare soil fitness for agricultural use under different managements in the Mediterranean environment. Soil Till. Res. 130, 91–98.
Bastida, F., Moreno, J.L., Hernandez, T., Garcia, C., 2006. Microbiological degradation index of soils in a semiarid climate. Soil Biol. Biochem. 38, 3463–3473.
Bhattacharyya, R., Prakash, V., Kundu, S., Gupta, H.S., 2006. Effect of tillage and crop rotations on pore size distribution and soil hydraulic conductivity in sandy clay loam soil of the Indian Himalayas. Soil Till. Res. 86, 129–140.
Bienes, R., Marques, M.J., Sastre, B., García-Díaz, A., Ruiz-Colmenero, M., 2016. Eleven years after shrub revegetation in semiarid eroded soils. Influence in soil properties. Geoderma 273, 106–114.
Chen, L., Huang, Z., Gong, J., Fu, B., Huang, Y., 2007. The effect of land cover/vegetation on soil water dynamic in the hilly area of the loess plateau, China. Catena 70, 200–208.
Chen, L., Wang, J., Wei, W., Fu, B., Wu, D., 2010. Effects of landscape restoration on soil water storage and water use in the Loess Plateau Region, China. For. Ecol. Manage. 259, 1291–1298.
Chen, Y., Wang, K., Lin, Y., Shi, W., Song, Y., He, X., 2015. Balancing green and grain trade. Nat. Geosci. 8, 739–741.
Clark, L.J., Whalley, W.R., Barraclough, P.B., 2003. How do roots penetrate strong soil? Plant Soil 255, 93–104.
Dal Ferro, N., Delmas, P., Duwig, C., Simonetti, G., Morari, F., 2012. Coupling X-ray microtomography and mercury intrusion porosimetry to quantify aggregate structures of a cambisol under different fertilisation treatments. Soil Till. Res. 119, 13–21.
Dal Ferro, N., Charrier, P., Morari, F., 2013. Dual-scale micro-CT assessment of soil structure in a long-term fertilization experiment. Geoderma 204–205, 84–93.
De Gryze, S., Jassogne, L., Six, J., Bossuyt, H., Wevers, M., Merckx, R., 2006. Pore structure changes during decomposition of fresh residue: x-ray tomography analyses. Geoderma 134, 82–96.
Deng, L., Shangguan, Z., 2012. Effects of the grain-for-green program on soil erosion in China. Int. J. Sediment Res. 27, 131–138.
Deng, L., Wang, K., Tang, Z., Shangguan, Z., 2016. Soil organic carbon dynamics following natural vegetation restoration: evidence from stable carbon isotopes (δ 13 C). Agric. Ecosyst. Environ. 221, 235–244.
Doube, M., Kłosowski, M.M., Argandacarreras, I., Cordelières, F.P., Dougherty, R.P., Jackson, J.S., Schmid, B., Hutchinson, J.R., Shefelbine, S.J., 2010. BoneJ: free and extensible bone image analysis in Image. J. Bone 47, 1076–1079.
Duan, L., Huang, M., Zhang, L., 2016. Differences in hydrological responses for different vegetation types on a steep slope on the Loess Plateau, China. J. Hydrol. 537, 356–366.
FAO-UNESCO, 1990. Soil map of the world: revised legend. World Soil Resources Report 60, Rome.
Fu, X., Shao, M., Wei, X., Horton, R., 2010. Soil organic carbon and total nitrogen as affected by vegetation types in Northern Loess Plateau of China. Geoderma 155, 31–35.
Garbout, A., Munkholm, L.J., Hansen, S.B., 2013. Temporal dynamics for soil aggregates determined using X-ray CT scanning. Geoderma 204–205, 15–22.
Hu, X., Li, Z.C., Li, X.Y., Liu, L.Y., 2016. Quantification of soil macropores under alpine vegetation using computed tomography in the Qinghai Lake Watershed, NE Qinghai-Tibet Plateau. Geoderma 264, 244–251.
Katuwal, S., Norgaard, T., Moldrup, P., Lamandé, M., Wildenschild, D., de Jonge, L.W., 2015. Linking air and water transport in intact soils to macropore characteristics inferred from X-ray computed tomography. Geoderma 237, 9–20.
Kravchenko, A.N., Wang, A.N.W., Smucker, A.J.M., Rivers, M.L., 2011. Long-term differences in tillage and land use affect intra-aggregate pore heterogeneity. Soil Sci. Soc. Am. J. 75, 1658–1666.
Le bissonnais, Y., 1996. Aggregate stability and assessment of soil crustability and erodibility.1: theory and methodology. Eur. J. Soil Sci. 47, 425–437.
Luo, L., Lin, H., Li, S., 2010. Quantification of 3-D soil macropore networks in different soil types and land uses using computed tomography. J. Hydrol. 393, 53–64.
Ma, R., Cai, C., Wang, J., Wang, T., Li, Z., Xiao, T., Peng, G., 2015. Partial least squares regression for linking aggregate pore characteristics to the detachment of undisturbed soil by simulating concentrated flow in Ultisols (subtropical China). J. Hydrol. 524, 44–52.
Marriott, C.A., Hudson, G., Hamilton, D., Neilson, R., Boag, B., Handley, L.L., Wishart, J., Scrimgeour, C.M., Robinson, D., 1997. Spatial variability of soil total C and N and their stable isotopes in an upland scottish grassland. Plant Soil 196, 151–162.
Masto, R.E., Chhonkar, P.K., Singh, D., Patra, A.K., 2008. Alternative soil quality indices for evaluating the effect of intensive cropping, fertilisation and manuring for 31 years in the semi-arid soils of India. Environ. Monit. Assess. 136, 419–435.
Pagliai, M., Vignozzi, N., Pellegrini, S., 2004. Soil structure and the effect of management practices. Soil Till. Res. 79, 131–143.
Papadopoulos, A., Bird, N.R.A., Whitmore, A.P., Mooney, S.J., 2009. Investigating the effects of organic and conventional management on soil aggregate stability using X-ray computed tomography. Eur. J. Soil Sci. 60, 360–368.
Peth, S., Horn, R., Beckmann, F., Donath, T., Smucker, A.J.M., Fischer, J., 2008. Three-dimensional quantification of intra-aggregate pore-space features using synchrotron-radiation-based microtomography. Soil Sci. Soc. Am. J. 72, 897–907.
Raiesi, F., Kabiri, V., 2016. Identification of soil quality indicators for assessing the effect of different tillage practices through a soil quality index in a semi-arid environment. Ecol. Indic. 71, 198–207.
Rasband, W.S., ImageJ. U.S. National Institutes of Health Bethesda, MD, USA.
Sinha, S., Masto, R.E., Ram, L.C., Selvi, V.A., Srivastava, N.K., Tripathi, R.C., George, J., 2009. Rhizosphere soil microbial index of tree species in a coal mining ecosystem. Soil Biol. Biochem. 41, 1824–1832.
Soil Survey Laboratory Methods Manual, 2004. http://soils.usda.gov/technical/lmm.
Sun, G., Zhou, G., Zhang, Z., Wei, X., Mcnulty, S.G., Vose, J.M., 2006. Potential water yield reduction due to forestation across China. J. Hydrol. 328, 548–558.
Udawatta, R.P., Anderson, S.H., 2008. CT-measured pore characteristics of surface and subsurface soils influenced by agroforestry and grass buffers. Geoderma 145, 381–389.
Udawatta, R.P., Anderson, S.H., Gantzer, C.J., Garrett, H.E., 2006. Agroforestry and grass buffer influence on macropore characteristics. Soil Sci. Soc. Am. J. 70, 1763–1773.
Udawatta, R.P., Anderson, S.H., Gantzer, C.J., Garrett, H.E., 2008. Influence of prairie restoration on CT-measured soil pore characteristics. J. Environ. Qual. 37, 219–228.
Wang, Z.J., Jiao, J.Y., Rayburg, S., Wang, Q.L., Su, Y., 2016. Soil erosion resistance of Grain for Green vegetation types under extreme rainfall conditions on the Loess Plateau, China. Catena 141, 109–116.
Zhang, Y.W., Shangguan, Z.P., 2016. The change of soil water storage in three land use types after 10 years on the Loess Plateau. Catena 147, 87–95.
Zhang, C., Liu, G., Xue, S., Song, Z., 2011. Rhizosphere soil microbial activity under different vegetation types on the Loess Plateau, China. Geoderma 161, 115–125.
Zhang, Y.W., Deng, L., Yan, W.M., Shangguan, Z.P., 2016. Interaction of soil water storage dynamics and long-term natural vegetation succession on the Loess Plateau, China. Catena 137, 52–60.
Zhao, S.W., Zhao, Y.G., Wu, J.S., 2010. Quantitative analysis of soil pores under natural vegetation successions on the Loess Plateau. Sci. China Earth Sci. 53, 617–625.
Zhao, D., Xu, M., Liu, G., Yao, X., Tuo, D., Zhang, R., Xiao, T., Peng, G., 2017. Quantification of soil aggregate microstructure on abandoned cropland during vegetative succession using synchrotron radiation-based micro-computed tomography. Soil Till. Res. 165, 239–246.
Zhou, H., Peng, X., Peth, S., Xiao, T.Q., 2012. Effects of vegetation restoration on soil aggregate microstructure quantified with synchrotron-based micro-computed tomography. Soil Till. Res. 124, 17–23.
Zhou, H., Peng, X., Perfect, E., Xiao, T., Peng, G., 2013. Effects of organic and inorganic fertilization on soil aggregation in an Ultisol as characterized by synchrotron based X-ray micro-computed tomography. Geoderma 195, 23–30.
Zhou, H., Fang, H., Mooney, S.J., Peng, X., 2016. Effects of long-term inorganic and organic fertilizations on the soil micro and macro structures of rice paddies. Geoderma 266, 66–74.